ABSTRACT

The thesis entitled **"*design and synthesis of organic materials having potential applications for OFET, Perovskites and OPV*"** has been divided into SIX chapters.

CHAPTER 1: Introduction. Chapter –1 is divided into 3 parts. Part-1 Introduction to OFET and part-2 is introduction to Perovskites and part-3 is introduction to OPV.

CHAPTER 2: A detailed study on the thermal, photo-physical, electrochemical properties and OFET applications of D-π-A-π-D structured unsymmetrical diketopyrrolopyrrole materials

CHAPTER 3: Simple and efficient dopant free hole transporting materials for perovskite solar cells with 13 % power conversion efficiency.

CHAPTER 4: Indacenodithiophene (IDT) based small molecule donor materials for small molecule organic photovoltaics.

CHAPTER 5: Small molecule donor materials having naphthadithiophene as a donor for bulk hetero junction solar cells.

CHAPTER 6: A Benzodithiophene based non-fullerene acceptors for Organic photovoltaic cells; effect of acceptor strength on optical, electro chemical and thermal properties.

The objective of this work is to understand how the chemical structures of molecules relate to their optical and electronic properties, and use this understanding to design and synthesize novel organic small molecules for Organic Field Effect Transistors OFETs) Perovskites and Organic Photovoltaics (OPV) applications.

The thesis entitled **"D*esign and synthesis of organic materials having potential applications for OFET, Perovskites and Organic photovoltaics*"** has been divided into SIX chapters. Chapter –1 is divided into 3 parts. Part–1 Introduction to OFET, part–2 is introduction to Perovskite solar cells and part–3 is introduction to OPV. Other chapters are further sub-divided into the following sections: Introduction, Results and discussions (Synthesis, Photo physical, electrochemical, thermal and photovoltaic/perovskite/OFET properties), Conclusions, Reference and Spectroscopic data.

Chapter 1

In 21st century, use of fossil energy, generated from non-renewable and polluting fossil fuels such as petroleum, coal, and natural gas has radically increased. As it's use rapidly increases compared to the rate of creation, the fossil fuel reserves may exhaust in near future. Hence, providing sustainable energy to mankind is one of the major challenges of the 21st century. According to the Kyoto Protocol, CO_2 emission must be reduced, and this should be done by using less fossil fuel. Hence, the CO_2 problem is another reason why new and renewable energy forms need to be considered. Our ability to meet the future needs of energy lies in the utilization of renewable sources. Among the several kinds of renewable energy sources like solar energy, wind power, hydroelectricity, bio-mass energy, geo-thermal power, and wave/tidal power solar energy is most promising as the sun delivers 165 thousand terawatt of power each day to the earth. It would be enough to feed our global energy hunger of 15 TW per year. To harvest the solar energy, photovoltaic (PV) technology is widely regarded as an ideal candidate to produce electricity from sun light. Organic solar cells (OSC) have been a promising next-generation green technology to address the increasing energy problems worldwide.

This chapter is divided into 3 parts. Part –1 introduces Organic Field Effect Transistors (OFETs), which includes, brief history, work principle, performance evolution system, device configuration and processing techniques, factors influencing the performance and some literature on P–type, n–type and ambipolar OFETs.

Part–2 introduces Perovskite solar cells, which includes, brief history, work principle, device configuration and processing techniques, hole transporting materials, dopant free hole transporting materials and some literature on hole transporting materials, and dopant free hole transporting materials.

Part–3 introduces the Organic Photovoltaics. Which includes a brief introduction of OSC, description of the operating principle of the OSC, photovoltaic technology, brief history of OSC, device architecture, device fabrication, about organic bulk heterojunction solar cells (BHJSC), working principle of BHJSC, photovoltaic parameters and literature reports on π-conjugated small molecules as donor materials for small molecule bulk heterojunction solar cells (SMBHJSC) and non-fullerene acceptors.

Chapter 2

Modulation of the molecular backbone with variations in their donor aromatic groups as end-capping units has a great impact not only for improving the molecular optoelectronic properties but also to control aggregation of the materials. Even though several DPP based small molecular semiconducting materials with symmetrical D-A-D architecture are reported, studies on the unsymmetrical DPP materials are very rare. Keeping this in mind, in this chapter we have design and synthesized a series of unsymmetrical DPP derivatives with different end capping units by anticipating that selection of appropriate end capping units can impart better properties compared to their symmetrical analogues. The synthesized unsymmetrical DPP materials have benzofuran at one end and chemical entities with different electron donating capacity and various extents of electronic conjugation are at the second side. Optoelectronic properties of the synthesized DPP derivatives are studied using UV-visible,

fluorescence, time resolved fluorescence spectroscopic techniques and cyclic voltammetry analysis. Molecular structures of the synthesized DPP-derivatives are shown in Scheme **2**. All the DPP-derivatives reported here contain benzofuran as one end-capping unit and they differ structurally only in use of other end-capping groups. The DPP-derivatives, **BFTPADPP, BFHTDPP** and **BFTFDPP** contain electron donating triphenylamine (TPA), 2-hexylthiophene (HT) and electron withdrawing p-trifluoromethylphenyl (TF) moieties, respectively as end-capping units and the derivatives **BFPhDPP, BFNaDPP, BFAnDPP** and **BFPyDPP** possess phenyl (Ph), naphthyl (Na), anthracenyl (An) and pyrenyl (Py) end groups that have various extents of electronic conjugation, respectively. A triple bond is introduced for the derivatives **BFPhDPP, BFNaDPP, BFAnDPP** and **BFPyDPP** by assuming that insertion of a triple bond can provide sufficient space to minimize the steric hindrance between the neighbouring moieties and helpful to improve the planarity of the materials.

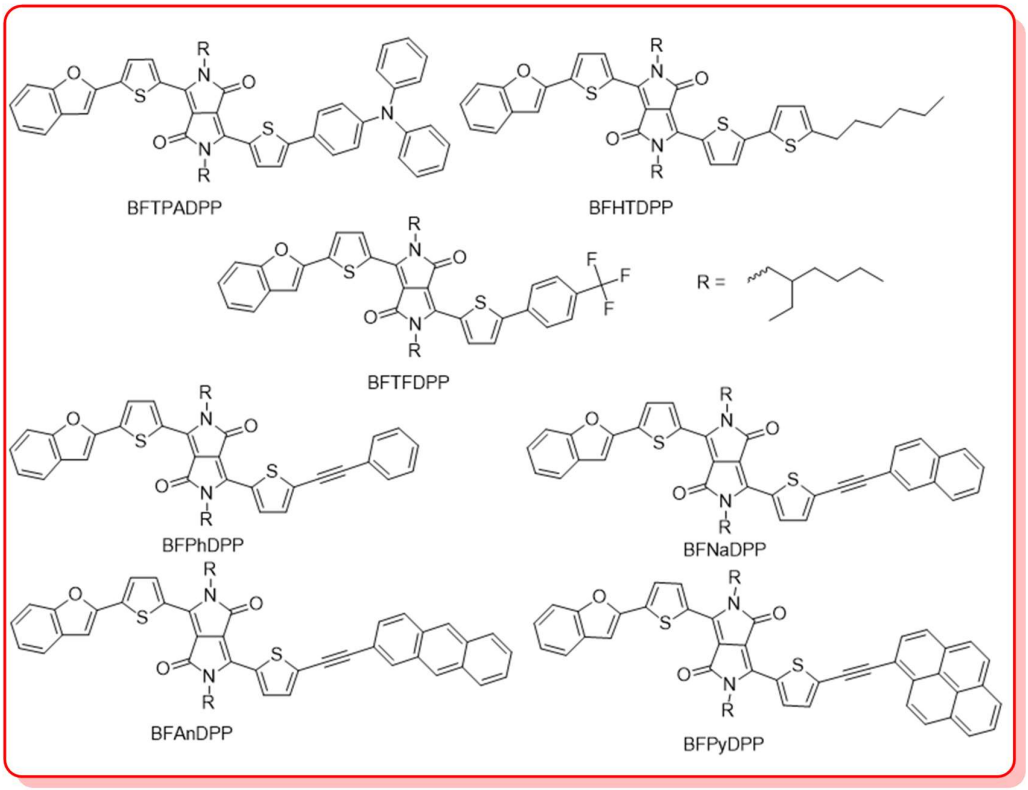

Scheme 2.1 Chemical structures of the synthesized DPP-derivatives.

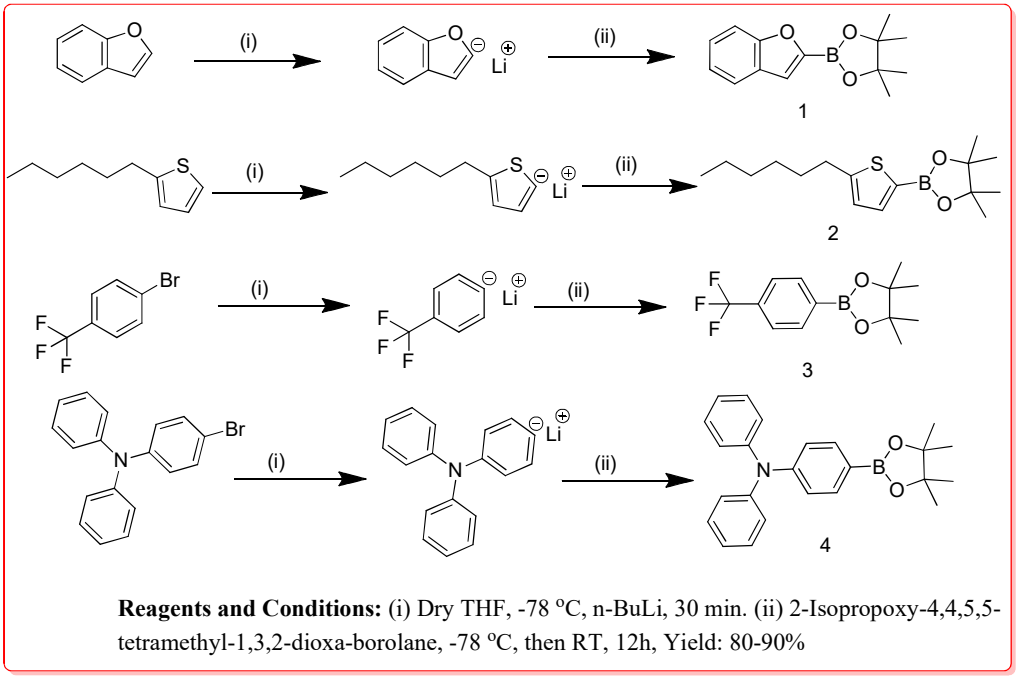

Reagents and Conditions: (i) Dry THF, -78 ºC, n-BuLi, 30 min. (ii) 2-Isopropoxy-4,4,5,5-tetramethyl-1,3,2-dioxa-borolane, -78 ºC, then RT, 12h, Yield: 80-90%

Scheme 2.2 Synthetic route for the preparation of intermediates **1, 2, 3** and **4**

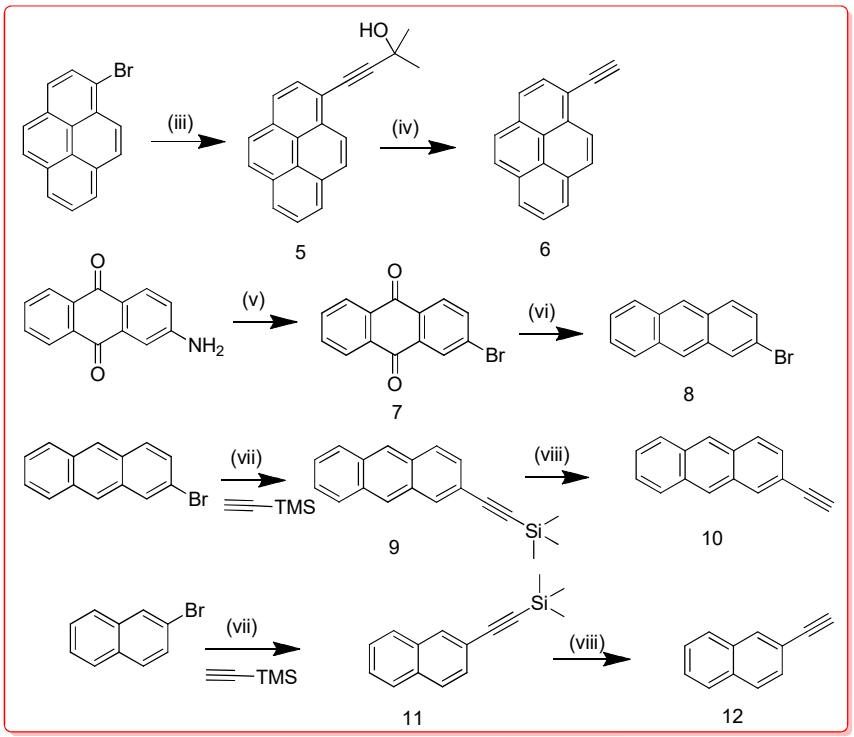

Scheme 2.3 Synthetic route for the preparation of intermediates **6, 10** and **12**

(iii) 2-methyl-3-buten-2-ol, CuI, triphenylphosphine, $Pd(dppf)Cl_2$.DCM, Dry toluene (1:1), Dry TEA, overnight. 84% (iv) KOH, Isopropanol 80 °C reflux 93% (v) $CuBr_2$, Isopentyl nitrite, 0 °C, Dry MeCN, 30 min, 1-2 hrs 31% (vi) (a) Dry THF, $NaBH_4$, 0 °C, 3 hrs, (b) $NaBH_4$, RT, 12 hr (c) H_2O, RT, 12 hrs, (d) 3M HCl, reflux, 6 hrs 22% (vii) $Pd(PPh_3)_2Cl_2$, CuI, TEA, 40 °C, 80% (viii) KOH, MeOH+DCM, (1:1), RT 90%.

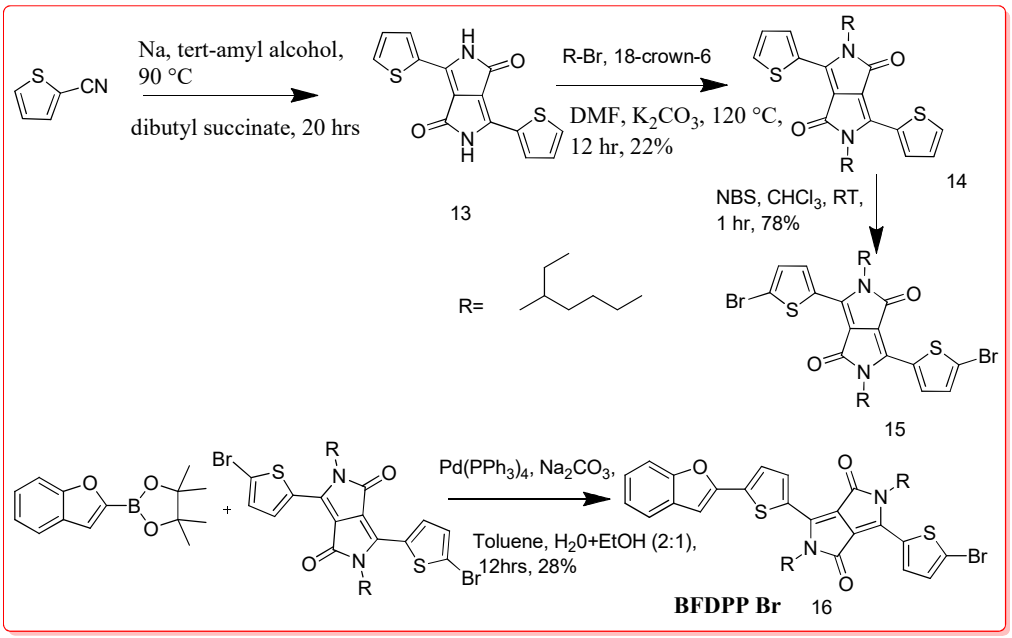

Scheme 2.4 Synthetic route for the **dibromo DPP (15)** and **BFDPPBr** intermediates

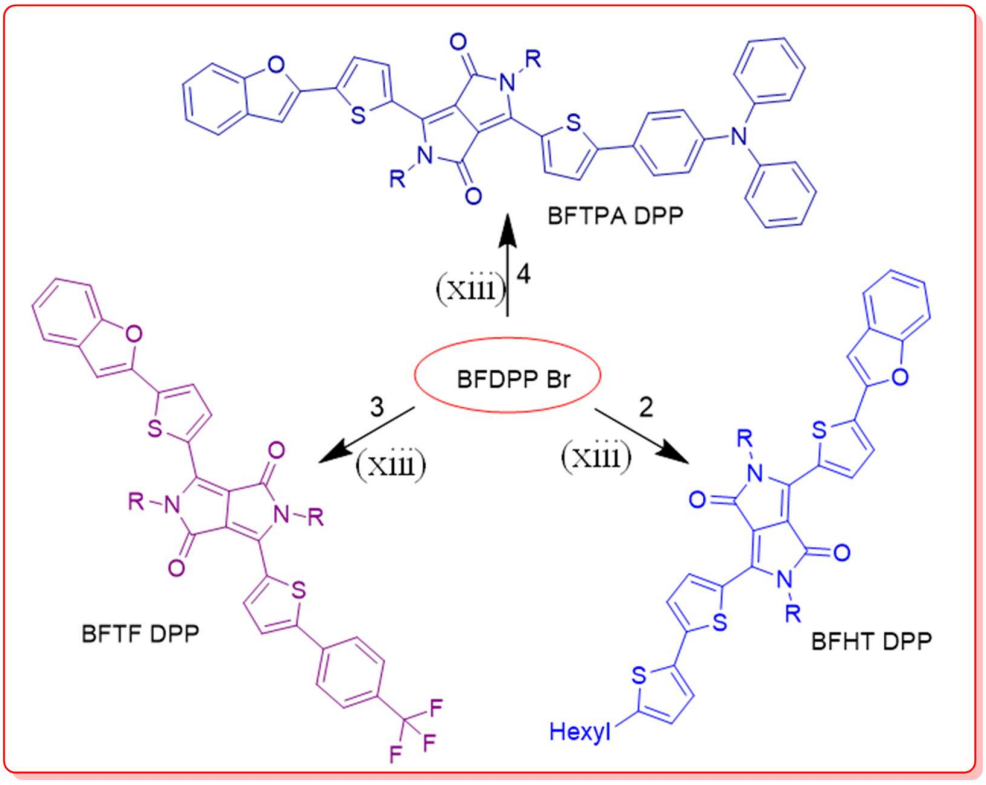

Scheme 2.5 Synthetic route for the target compounds (**BFTPA DPP, BFHT DPP** and **BFTF DPP**)

Reagents and Conditions: (xiii) Toluene, $Pd(PPh_3)_4$, Na_2CO_3, H_2O+EtOH (2:1), 12h, 70-75%. R = Ethyl Hexyl.

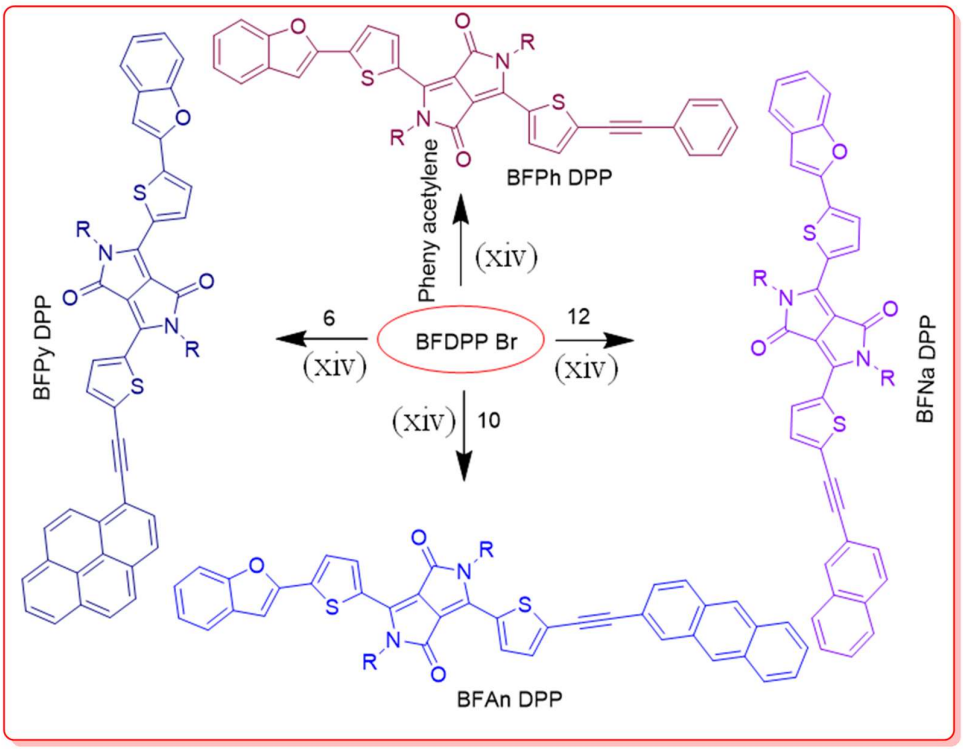

Scheme 2.6 Synthetic route for the target compounds (**BFPh DPP, BFNa DPP, BFAn DPP** and **BFPy DPP**)

Reagents and Conditions: (vix) Toluene, $Pd(PPh_3)_2Cl_2$, CuI, Diisopropyl amine, reflux, 12h, 80-85% R = Ethyl Hexyl.

The UV-visible absorption characteristics of the reported DPP-derivatives were measured in both solution and thin film states. The UV-visible absorption spectra of these materials in chloroform solution and the corresponding data is provided in Table 2.1.

Table 2.1 UV-visible absorption, Emission, (solution), thin film, and band gap data of the synthesized DPP-derivatives of the synthesized DPP-derivatives.

Compound Code	λ_{abs} (nm)	ε (L M^{-1} Cm^{-1})	λ_{abs}film (nm)
BFTPADPP	592, 631	57832, 64008	594, 689
BFHTDPP	584, 627	38911, 41732	591, 660
BFTFDPP	573, 613	33600, 35230	582, 652
BFPhDPP	569, 612	48670, 52026	587, 654
BFNaDPP	573, 616	39302, 41752	595, 654
BFAnDPP	576, 619	37532, 39961	602, 658
BFPyDPP	582, 623	50255, 53241	597, 679

The oxidation potentials, HOMO, LUMO, and electrochemical band gap values were summarized in Table 2.2. **BFTPADPP, BFHTDPP**, **BFTFDPP, BFPhDPP, BFNaDPP, BFAnDPP** and **BFPyDPP** were shown 0.67 and 0.82 V onset oxidation potential values respectively.

Table 2.2 Oxidation potential (E_{ox}), reduction potential (E_{red}), HOMO, LUMO and electrochemical band gap (E_g) of the compounds.

Compound code	$E_{+1/2}^{+/0}$ (V)	HOMO (eV)[a]	$E_{1/2}^{0/-}$ (V)	LUMO (ev)[b]	Band gap[c] (eV)
BFTPADPP	0.67	-5.07	-0.99	-3.41	1.66
BFHTDPP	0.72	-5.12	-0.96	-3.44	1.68
BFTFDPP	0.81	-5.21	-0.94	-3.46	1.75
BFPhDPP	0.85	-5.25	-0.98	-3.42	1.83
BFNaDPP	0.84	-5.24	-0.94	-3.46	1.78
BFAnDPP	0.83	-5.23	-0.93	-3.47	1.76
BFPyDPP	0.82	-5.22	-0.91	-3.49	1.73

To evaluate the thermal properties for **BFTPADPP, BFHTDPP**, **BFTFDPP, BFPhDPP, BFNaDPP, BFAnDPP** and **BFPyDPP**, thermo gravimetric analysis (TGA) measurements were performed under nitrogen atmosphere at a heating rate of 10 ℃ per minute. The corresponding data are summarized in **Table 2.3.** All the synthesized materials showed the decomposition temperatures (T_d, defined as that at which 5 wt % loss is observed) above ~348 ℃. This observation clearly indicates good thermal stability of these materials even at high temperatures, required for vacuum deposition.

Table 2.3 Thermal data of the Synthesized DPP compounds

Compound code	T_d (℃)	T_m (℃)
BFTPADPP	373.5	190.3
BFHTDPP	348.7	140.1
BFTFDPP	352.4	207.0
BFPhDPP	364.8	121.7
BFNaDPP	387.2	185.3
BFAnDPP	390.9	-
BFPyDPP	379.7	193.7

The charge transport properties of the synthesized DPP derivatives were measured in organic field-effect transistors (OFETs). The device configuration was bottom gate bottom contact with gold electrodes as source and drain contacts. The gate dielectric was 230 nm thick SiO_2. All the synthesized DPP derivatives showed moderate to good hole transporting ability and among all these derivatives, highest hole mobility was measured for BFPyDPP (6.7 x 10^{-4} cm^2/Vs) with VT of -9 V (packing between the molecules due to the presence of flat pyrene as one terminal moiety. The OFET parameters for these DPP derivatives are summarized in Table 2.4.

Table 2.4 Field-effect transistor data of the synthesized DPP-derivatives

Material code	Mobility(cm^2/Vs) saturation regime	Mobility(cm^2/Vs) Linear regime	V_T (V)	$I_{on/off}$
BFTPADPP	8.85 x 10^{-5}	4.95 x 10^{-5}	-5	2.02 x10^2
BFHTDPP	1.12 x 10^{-4}	1.02 x 10^{-4}	-20	9.17 x10^2
BFTFDPP	2.25 x 10^{-5}	1.35 x 10^{-5}	-38	3.01 x10^2
BFPhDPP	2.16 x 10^{-4}	2.02 x 10^{-4}	-18	1.12 x10^2
BFNaDPP	2.70 x 10^{-5}	4.22 x 10^{-5}	-11	7.92 x10^1
BFAnDPP	4.72 x 10^{-6}	3.37 x 10^{-6}	-10	8.30 x10^2
BFPyDPP	6.74 x 10^{-4}	4.11 x 10^{-4}	-9	7.02 x10^1

In conclusion, seven unsymmetrical DPP-derivatives namely BFTPADPP, BFHTDPP, BFTFDPP, BFPhDPP, BFNaDPP, BFAnDPP and BFPyDPP with D-π-A-π-D architecture have been synthesized and their optoelectronic properties are measured and the effect of end capping units on their optoelectronic properties is explored. The obtained values are compared with their symmetrical analogue dibenzofuran-DPP DPP(TBFu)$_2$. All the synthesized derivatives show improved UV and visible region light harvesting ability compared to DPP(TBFu)$_2$. The estimated HOMO and LUMO energy levels of the synthesized materials agree with the work functions of the most commonly used cathode materials (Au and Ag) and as well as with the fullerene acceptors ($PC_{60}BM$ and $PC_{70}BM$). OFETs are fabricated using these materials and they show moderate to good charge carrier mobilities. Among the OFETS fabricated, OFETs with BFPyDPP exhibited the best performance characteristics with the hole mobility of 6.7 x10^{-4} cm^2/Vs with VT of -9 V and the observed mobility is four times better compared to OFETs with DPP(TBFu)$_2$. Excellent thermal stability, good light harvesting capacity with appropriate energy levels and good charge carrier mobilities designated the utility of these materials in various applications like organic BHJ solar cells, disposable electronics and biomedical devices.

Chapter 3

During the last couple of years extensive investigations have been made to improve the PCE of perovskite solar cells by engineering the structures of hole and electron transporting materials, by varying the perovskite material composition and modifying the fabrication conditions. Particularly, development of new hole transporting materials (HTMs) has been emerged as one of the thirsty areas of research. Various hole transporting materials like metal-phthalocyanines, organic polymers and small molecule materials are reported for PSCs. Among the all, 2,2',7,7'-tetrakis(*N,N*-bis(*p*-methoxyphenyl) amino)-9,9'-spirobifluorene (spiro-OMeTAD) is acquired a special place and PCE of 20.8% is reported for the PSCs by adopting suitable fabrication procedures. However, tedious procedure for the synthesis and high production cast associated with spiro-OMeTAD hinder its practical applicability and denotes the necessity to develop new alternates for spiro-OMeTAD. Recently, dopant-free hole transporting materials have attained great importance as they eliminate the usage of dopants or additives and thereby by overcome the disadvantages of poor device stability and unwanted ionic migrations and interactions associated with dopants added to HTMs. Apart from the advantages, most of the reported dopant-free HTMs for PSCs suffer from the drawbacks like tedious and extensive synthesis and purification procedures, which limits their widespread applications.

Keeping all these points in mind, we have synthesized two new small molecular D-A conjugate materials, **DTP 1M**, **DTP 2M and DTP 3M**, with D-π-A architecture having dithieno[3,2-*b*:2',3'-*d*]pyrrole (DTP) as donor, dicyanovinylene as acceptor and thiophene (**DTP 1M**), thiazole (**DTP 2M**) and phenyl (**DTP 3M**) as spacer moieties and successfully applied them as HTMs for PSCs, to identify the effect of spacer unit.

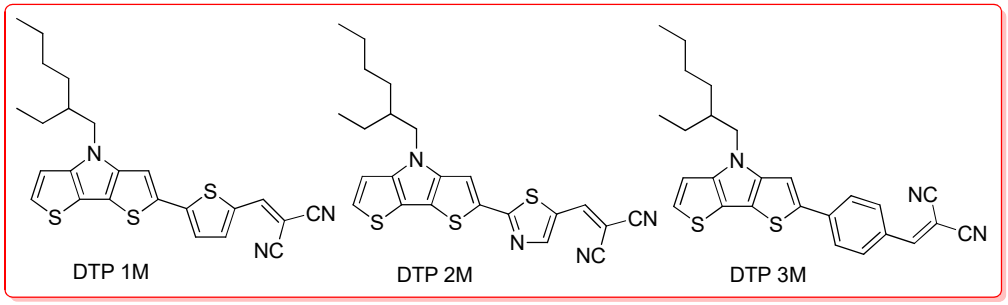

Scheme 3.1 Chemical structures of the target molecules

In this respect, oligomers **DTP 1M**, **DTP 2M and DTP 3M** were designed such that solubilizing side chains were introduced at the central nitrogen (2-ethylhexyl). Keeping dithienopyrrol moiety (donor) and dicyanovinylene (acceptor), common, we have varied the spacer. Three types of spacers were used, which are thiophene, (**DTP 1M**) thiazole (**DTP 2M**) and phenyl (**DTP 3M**).

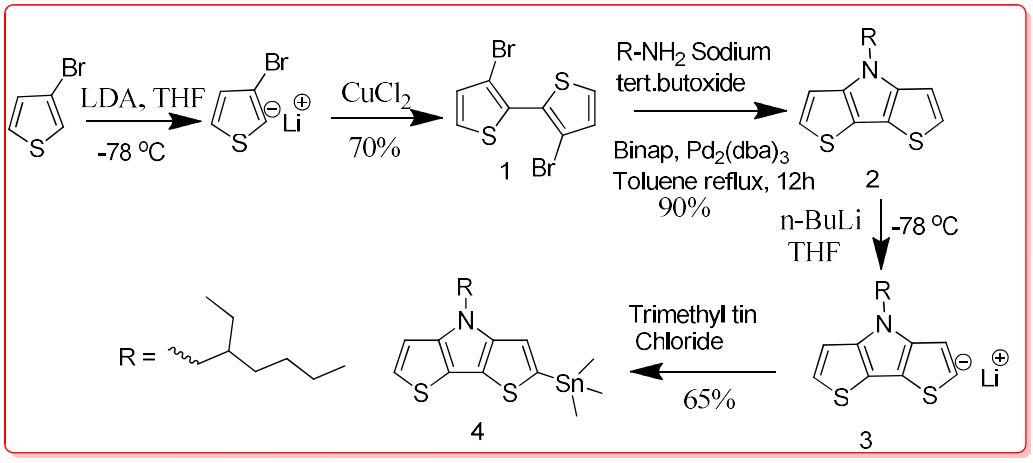

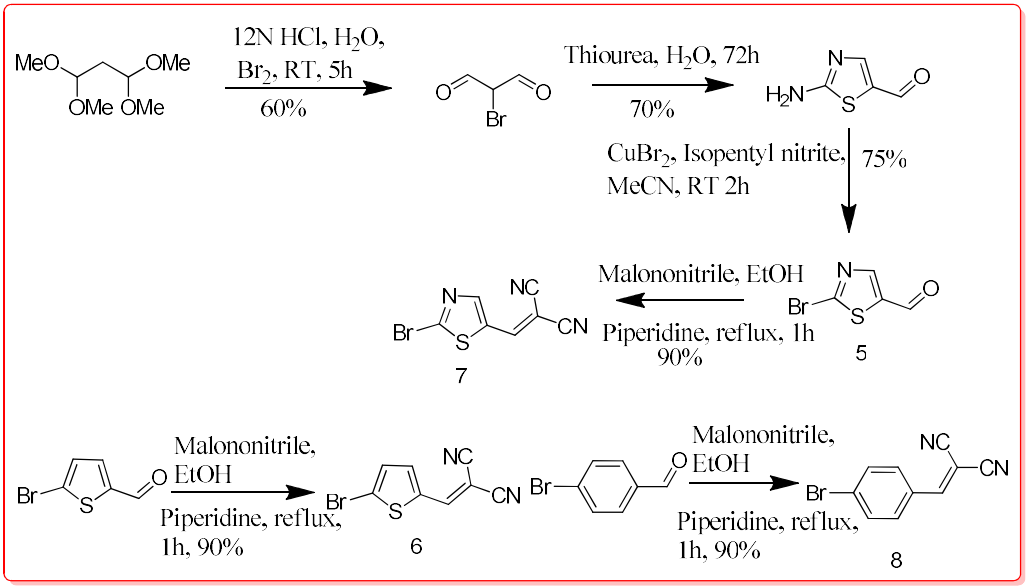

Scheme 3.2 Synthetic route for the preparation intermediates

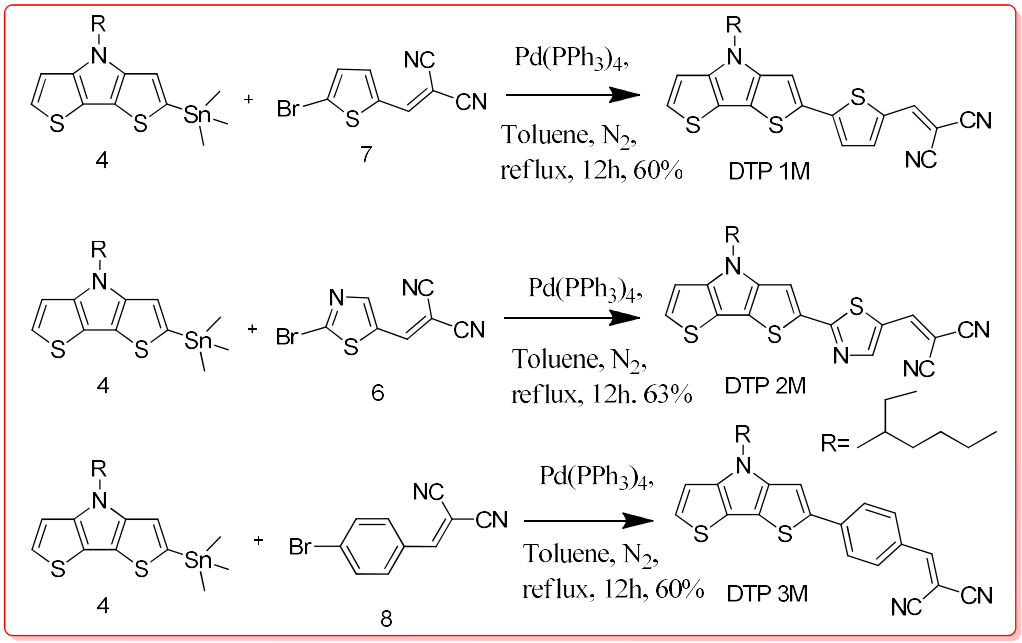

Scheme 3.3 Synthetic route for the preparation of **DTP 1M, DTP 2M** and **DTP 3M**

The UV-visible absorption spectra of **DTP 1M, DTP 2M,** and **DTP 3M** have absorption bands ranging 260-625 nm. The absorption spectra of these three compounds recorded in chloroform ($1x10^{-5}$ M). The bathochromic shift of 37 nm and

41 nm in absorption maxima is observed for **DTP 3M to DTP 2M**, and **DTP 3M to DTP 1M** nm respectively, and 5 nm red shift is observed for **DTP 2M to DTP 1M**, and the results are listed in Table 3.1.

Table 3.1 Absorption (λ_{abs} in nm), molar extinction coefficient (ε), of **DTP 1M, DTP 2M,** and **DTP 3M** recorded in chloroform**.**

Compound code	λ_{abs} (nm)	Molar extinction coefficient (ε) L M^{-1} cm^{-1}	λ_{fluo} (nm)	Optical band gap (eV)
DTP 1M	340, 540	46755	618	2.10
DTP 2M	335, 536	53809	608	2.07
DTP 3M	322, 499	49374	607	2.24

The derivatives have their oxidation potentials in the range of 0.90–1.00 eV. The HOMO/LUMO values for **DTP 1M, DTP 2M,** and **DTP 3M** were calculated as -5.30/-3.19, -5.40/ -3.25, and -5.36/-3.13 eV, respectively. The insertion of thiazole unit in oligomer **DTP 2M** resulted in positive shift in oxidation potentials compared to **DTP 1M** (DTP 1M having thiophene unit as a spacer). HOMO, LUMO, and optical band gap values are summarized in Table 3.2.

Table 3.2 Electrochemical data of **DTP 1M, DTP 2M,** and **DTP 3M**

Compound code	E_{ox}^{onset} (volts)[a]	HOMO[b]	LUMO[c]	E_g^{opt}(eV)
DTP 1M	0.90	-5.30	-3.19	2.11
DTP 2M	1.00	-5.40	-3.25	2.25
DTP 3M	0.96	-5.36	-3.13	2.23

To evaluate the thermal properties for new hole transporting materials (HTMs) **DTP 1M** and **DTP 2M,** thermo-gravimetric analysis (TGA) measurements were performed

under nitrogen atmosphere at a heating rate of 10 °C per minute. The representative data was summarized in Table 3.3.

Table 3.3 Thermal data of **DTP 1M** and **DTP 2M**

compound	T_d [a] (°C)	T_m [b] (°C)
DTP 1M	332	138
DTP 2M	329	169

[a] T_d: decomposition temperature (corresponding to 5% weight loss). T_m [b]: melting point temperature.

Perovskite solar cells (PSCs) with the conventional structure of FTO/TiO_2/MesoTiO_2/$MeAPbI_3$/HTM/Ag were fabricated. PSCs employing spiro-OMeTAD with 4-tert-butylpyridine and Bis-(trifluoromethane) sulfonimide lithium salt as HTM were also fabricated, Devices with **DTP 1M** and **DTP 2M** show superior photovoltaic performance (PCE 13.95 % and 12.52 %, respectively for the devices based on **DTP 1M** and **DTP 2M**) with higher J_{SC}, V_{OC} and FF values (J_{SC}, V_{OC} and FF values are 24.99 mA/cm^2, 0.94 V, 0.594 and 19.41 mA/cm^2, 0.97 V, 0.665, respectively for the PSCs with **DTP 1M** and **DTP 2M** HTMs) compared to the devices employing spiro-OMeTAD (PCE 7.67 %, J_{SC}, V_{OC} and FF values are 17.17 mA/cm^2, 0.74 V and 0.603) as HTM. The higher V_{OC} values for **DTP 1M** and **DTP 2M**-based devices are expected because of the deeper HOMO energy levels of **DTP 1M** and **DTP 2M** than that of spiro-OMeTAD. Corresponding Photovoltaic parameters of the perovskite solar cell devices listed in table 3.4.

Table 3.4 Photovoltaic parameters of the perovskite solar cell devices based on **DTP 1M**, **DTP 2M** and spiro-OMeTAD**.**

HTM	J_{SC} (mA/cm^2)	V_{OC} (V)	FF	PCE (%)
DTP 1M	24.99	0.94	0.594	13.95
DTP 2M	19.41	0.97	0.665	12.52
Spiro-OMeTAD	17.17	0.74	0.603	7.67

In conclusion, we have synthesized two multichromophoric hybrid small molecules with D-π-A architecture (**ICTH1** and **ICTH2**) and explored their photophysical, electrochemical and thermal properties. Perovskite solar cells were fabricated using **ICTH1** and **ICTH2** as the hole transporting materials without using any dopants and PCEs of 13.95 and 12.52 % were achieved respectively. The observed PCE of the devices outperforms the spiro-OMeTAD-based devices (PCE 7.67 %). Synthetic simplicity, low production cost and dopant-free application of **ICTH1** and **ICTH2** in solar cell fabrication signify the potentiality of these materials over the conventional spiro-OMeTAD HTM.

Chapter 4

In the past few years researchers much interested on Bulk hetero junction solar cells (BHJSCs) due to their advantages low cost, light weight, flexibility, and solution procesability**.** Over the last few decades polymer solar cells power conversion efficiencies over ≥10% have been achieved, it is mainly due to optimizing the polymer molecular backbone and device architecture. Compare with polymer solar cells (PSCs) small molecule organic solar cells (SMOSCs) having numerous advantages like simple synthesis and purification, monodispersity, well defined molecular structure and weight, no end group contaminants, easy to tune the energy levels by changing the molecular backbone and good reproducibility. SMOSCs based on their donor material configuration classified into three types, i.e. Donor-Acceptor-Donor (D-A-D), Donor/Donor^1-Acceptor-Donor/ Donor^1 (D/D^1-A-D-A-D/ D^1), Acceptor-Donor-Acceptor (A-D-A). Among all of three A-D-A type small molecules shows good performance in small molecule organic solar cells (SMOSCs). This type of materials

easily tunes the HOMO/LUMO energy levels, optical properties by changing the central donor, acceptor, and spacer.

In this chapter we design and synthesized two new A-D_1-D_2-D_1-A architecture donor materials named **IDT Rh** and **IDT ID** for applications in small molecule organic solar cells. Both molecules having central indaceno[2,1-b:6,5-b′]dithiophene (IDT) donor (D_2) and dithieno[3,2-b:2',3'-d]pyrrole as D_1 donor, differ with their terminal acceptor moiety (Rhodanine for **IDT Rh** and 1,3-indane di one for **IDT ID**) to studied the effect of acceptor unit on optical, electro chemical and thermal properties of donor material. They are good solubility in common organic solvents like chloroform.

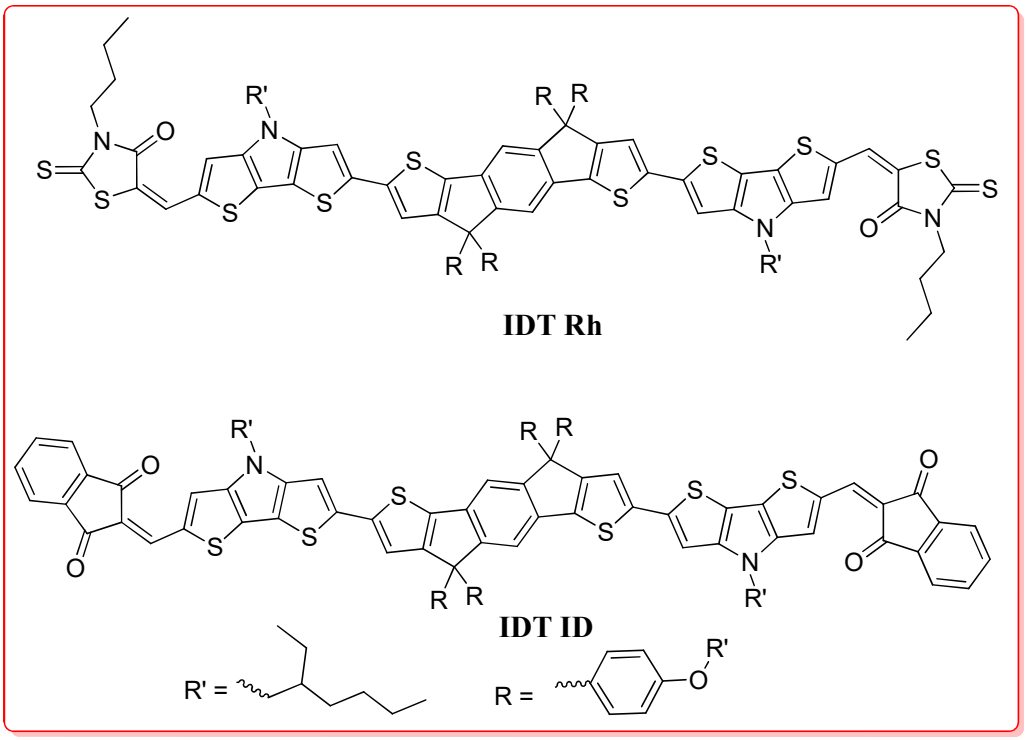

Scheme 4.1 Chemical structures of the target molecules

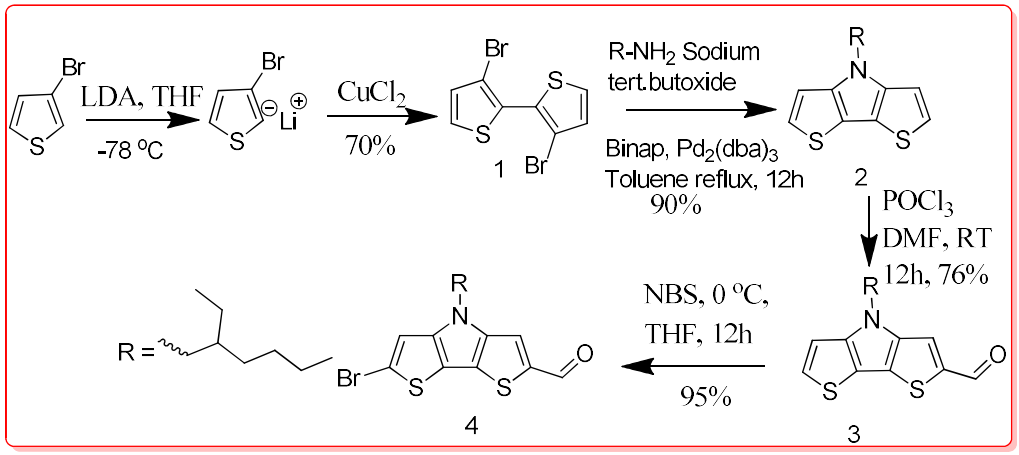

Scheme 4.2 Synthetic route for the preparation of **2, 3, 4**

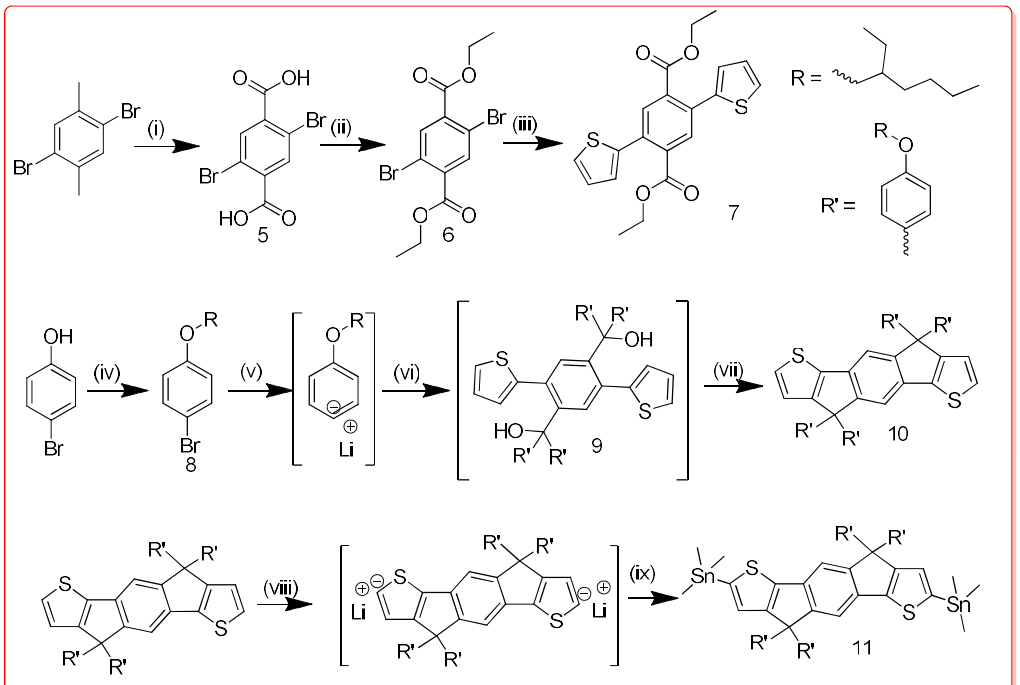

Reagents and conditions: (i) $KMnO_4$, H_2O + t-BuOH (1:1), reflux, 18h (ii) EtOH, H_2SO_4, reflux, overnight (iii) tributyl(thiophen-2-yl)stannane, $Pd(PPh_3)_4$, Toluene, reflux, 12h (iv) K_2CO_3, 2-ethyl hexyl bromide, DMF, 80 °C, overnight (v) n-BuLi, -78 °C, THF (vi) Compound 7, RT, overnight (vii) H_2SO_4, Acetic acid, reflux, 2h (xiii) n-BuLi, -78 °C, THF (ix) Trimethyl tin chloride

Scheme 4.3 Synthetic route for the preparation of **5, 6, 7, 8, 10 and 11.**

12 synthesized via Pd^0 catalyzed stille cross coupling reaction between bis stannylated intermediate (11) and bromo aldehyde intermediate (4).

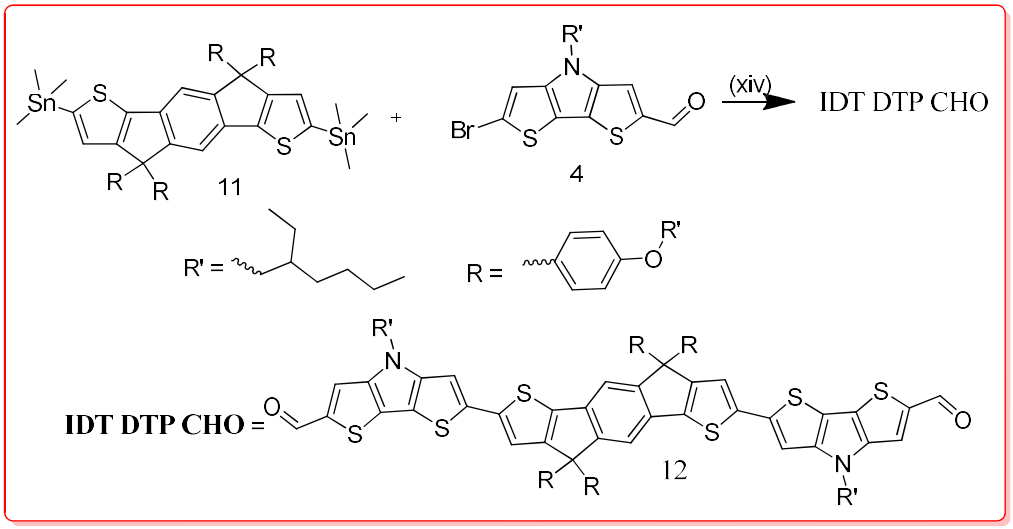

Scheme 4.5 Synthetic route for the preparation of **12**

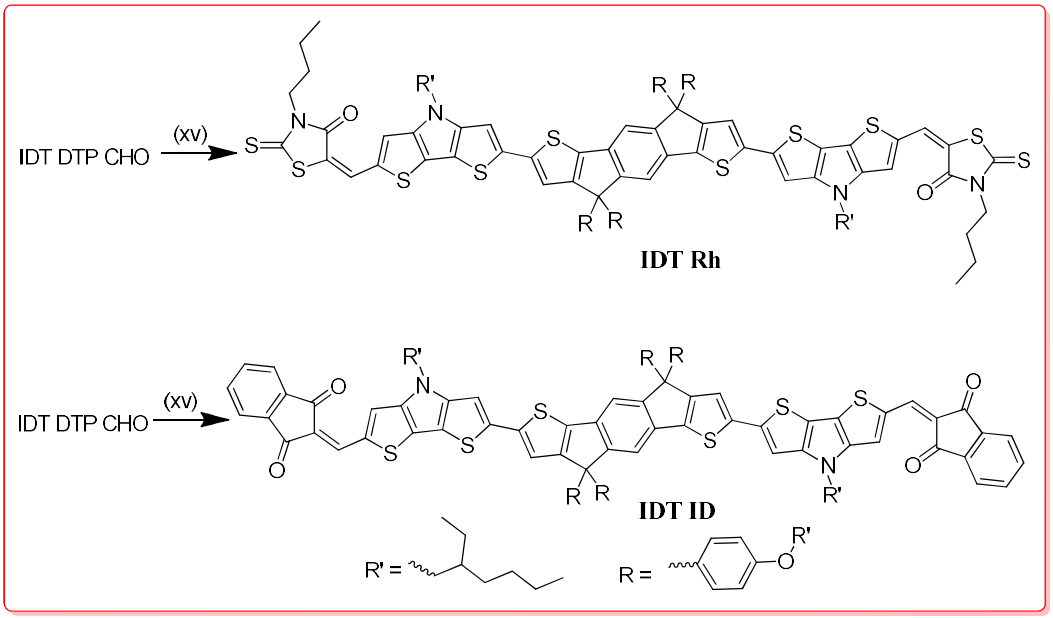

Scheme 4.6 Synthetic route for the target compounds (**IDTP Rh** and **IDTP ID**)

The target molecules prepared by knoevenagel condensation of **12** with butyl rhodanine and 1,3-indanedione for **IDT Rh** and **IDT ID** respectively. both reactions carried out at reflux temperature under N_2 conditions.

The UV–Visible absorption spectra of two new small molecule donor materials were recorded in $CHCl_3$ solution at 10^{-5} M concentration. They are showing two absorption

bands, one is in visible region (500 nm-750 nm), IDT ID oligomer shows a red shift of 22 nm than IDT Rh oligomer but slight decreasing in absorption intensity. The absorption edge [λ_{edge}] of the solution (both UV-Visible and fluorescence in solution state) is 655 nm and 668 nm, based on above data the optical band gap of oligomers IDT Rh and IDT ID are 1.89 and 1.85 respectively. (optical band gap calculated by using Formula 1240/λ_{edge}). Fluorescence emission spectra of **IDT Rh and IDT ID** ($1x10^{-5}$ M) in $CHCl_3$ are depicted and the results are summarized in Table **4.1**. **IDT Rh and IDT ID** displayed emission maxima at 704 and 708 nm respectively.

Table 4.1 Absorption maximum (λ_{abs} in nm), molar extinction coefficient (ε), fluorescence and Optical band gap of synthesized compounds

Compound code	λ_{abs} **(nm)**	**Molar extinction coefficient (ε , M^{-1} cm^{-1})**	λ_{fluo} **(nm)**	**Optical band gap (E_g^{opt})**
IDT Rh	441, 607	113075	704	1.89
IDT ID	474, 629	99397	708	1.84

To identify the relationship between the chemical structures and electrochemical properties of **IDT Rh, IDT ID** by cyclic voltammetry. IDT Rh and IDT ID both compounds exhibit irreversible oxidation waves and the oxidation potentials are 0.65 and 0.63 V for IDT Rh and IDT ID, corresponding data provided in table 4.1

Table 4.2 Electrochemical data of **IDT Rh** and **IDT ID**

Compound code	E_{ox}^{onset} **(volts)[a]**	**HOMO[b]**	**LUMO[c]**	ΔE_g^{opt} **[d](eV)**
IDT Rh	0.65	5.35	3.46	1.89
IDT ID	0.63	5.33	3.49	1.84

To evaluate the thermal properties for two new IDT based small molecule donor materials (**IDT Rh and IDT ID**), thermogravimetric analysis (TGA) measurements were performed under nitrogen atmosphere at a heating rate of 10 ℃ per minute. The

representative TGA data were summarized in Table 4.3. Thermal decomposition temperatures (T_d) corresponding to 5% weight loss of these compounds were in 422 ℃ and 412 ℃ for **IDT Rh** and **IDT ID**.

Table 4.3 Thermal properties of synthesized donor materials

Compound Code	T_d [a] (℃)
IDT Rh	422
IDT ID	412

[a] T_d: decomposition temperature (corresponding to 5% weight loss).

To evaluate the photovoltaic properties of **IDT ID**, bulk heterojunction solar cells were fabricated using **IDT ID** as donor and $PC_{71}BM$ as acceptor materials with a conventional device structure of ITO/PEDOT: PSS/ **IDT ID**: $PC_{71}BM$/PFN/Al. Initially, BHJSCs were optimized by fabricating the devices with various D/A weight ratios of 1:1, 1: 1.5 in chloroform and 1:1, 1: 1.5, and 1: 2 in Chlorobenzene solution keeping the total concentration as 16 mg mL^{-1}. We found that devices based on **IDT ID**: $PC_{71}BM$ (1: 2 wt ratio) show best photovoltaic performance. The device fabricated from the active layer processed with chloroform solution showed a PCE of 1.18% with a J_{SC} of 4.64 mA cm^{-2}, a V_{OC} of 0.79 V and a FF of 0.32 (1: 1.5 ratio of donor and acceptor), and the device fabricated from the active layer processed with chlorobenzene solution showed a PCE of 2.05% with a J_{SC} of 7.47 mA cm^{-2}, a V_{OC} of 0.76 V and a FF of 0.36 (1: 2 ratios of donor and acceptor). The overall PCE of the solar cell based on **IDT ID: $PC_{71}BM$** processed with chloroform is quite low and it could be due to the poor J_{SC} and FF associated with these devices. Fabricating BHJSCs based on the thermal annealed (TA) and thermal followed by solvent vapour annealed (TA + SVA) active layers has no effect on power conversion efficiency.

Table 4.4 Photovoltaic parameters of the BHJSC devices based on **IDT ID**

Active la yer	Process Solvent	D: A ratio	V_{OC} (V)	J_{SC} (mA cm^{-2})	FF	PCE_{max} (PCE_{avg}) (%)
IDTID: P $C_{71}BM$	CF	1.0:1.0	0.77	4.39	0.30	1.02 (0.81)
	CF	1.0:1.5	0.79	4.64	0.32	1.18 (0.85)
	CB	1.0:1.0	0.76	3.89	0.28	0.82 (0.76)
	CB	1.0:1.5	0.72	6.19	0.34	1.51 (1.46)
	CB	1.0:2.0	0.76	7.47	0.36	2.05 (1.98)

In conclusion, we have designed and synthesized two new **IDT** based small molecules *i.e* **IDT Rh** and **IDT ID** were synthesized. Both compounds having Indacenodithiophene as a central donor and dithienopyrrole as another donor and by changing in the acceptor *i.e.* rhodanine (for **IDT Rh**) to 1,3-indanedione (for **IDT ID**), to evaluate the effect of acceptor on optical, electro chemical and thermal properties, as well as application in SMBHJSCs. Bulk heterojunction solar cells were fabricated using **IDT ID** as donor and $PC_{71}BM$ as acceptor materials with a conventional device structure of ITO/PEDOT: PSS/ **IDT ID**: $PC_{71}BM$/PFN/Al. The device fabricated from the active layer processed with chloroform solution showed a PCE of 1.18% with a J_{SC} of 4.64 mA cm^{-2}, a V_{OC} of 0.79 V and a FF of 0.32 (1: 1.5 ratio of donor and acceptor), and the device fabricated from the active layer processed with chlorobenzene solution showed a PCE of 2.05% with a J_{SC} of 7.47 mA cm^{-2}, a V_{OC} of 0.76 V and a FF of 0.36 (1: 2 ratios of donor and acceptor). The high V_{OC} of device is due the deeper HOMO energy level (-5.33) of **IDT ID** donor.

Chapter 5

Small molecule organic solar cells having several advantages like good solubility in common organic solvents, high open circuit voltage, batch-to-batch variability in polymer solar cells is difficult, but small molecules have well defined

molecular structure, which can alleviate issues of polymer solar cells. Small molecules also have some disadvantages which are, they exhibit inferior film quality its leads to lower J_{SC}, less thermal stability than the polymer counterparts. For the design of SM donors, it generally highlights (i) efficient and broad optical absorption, (ii) low lying HOMO energy levels, (iii) planar structures with good inter molecular contacts, and (iv) solubility more than 10 mg/mL.

Optimization of donor material according to the acceptor material (PCBM or Fullerene free acceptor) is a strategy to improve power conversion efficiencies (PCEs) of small molecule bulk heterojunction solar cells (SMBHJSCs). Based on that here we designed and synthesized two donor molecules **NDT Rh** and **NDT ID** by varied in acceptor group (Butyl rhodhanine for **NDT Rh** and 1,3-Inadanedione for **NDT ID**) for small molecule donor materials with A-D'-D-D'-A architecture. Central donor is naphtho[2,1-b:3,4-b']dithiophene (NDT), dithieno[3,2-b:2′,3′-d]pyrrole (DTP) donor located into adjacent to the acceptor. Introduced the Ethyl hexyl groups on naphtho[2,1-b:3,4-b']dithiophene (NDT), dithieno[3,2-b:2′,3′-d]pyrrole (DTP) to improve the solubility of donor materials.

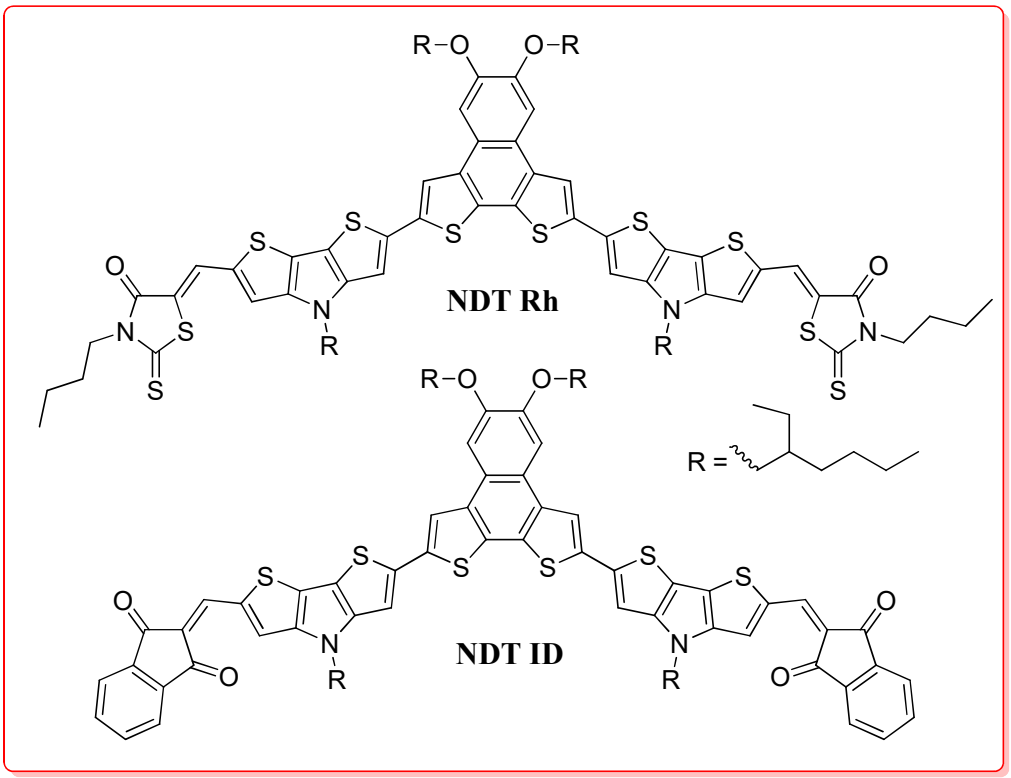

Scheme 5.1 Chemical structures of the target molecules

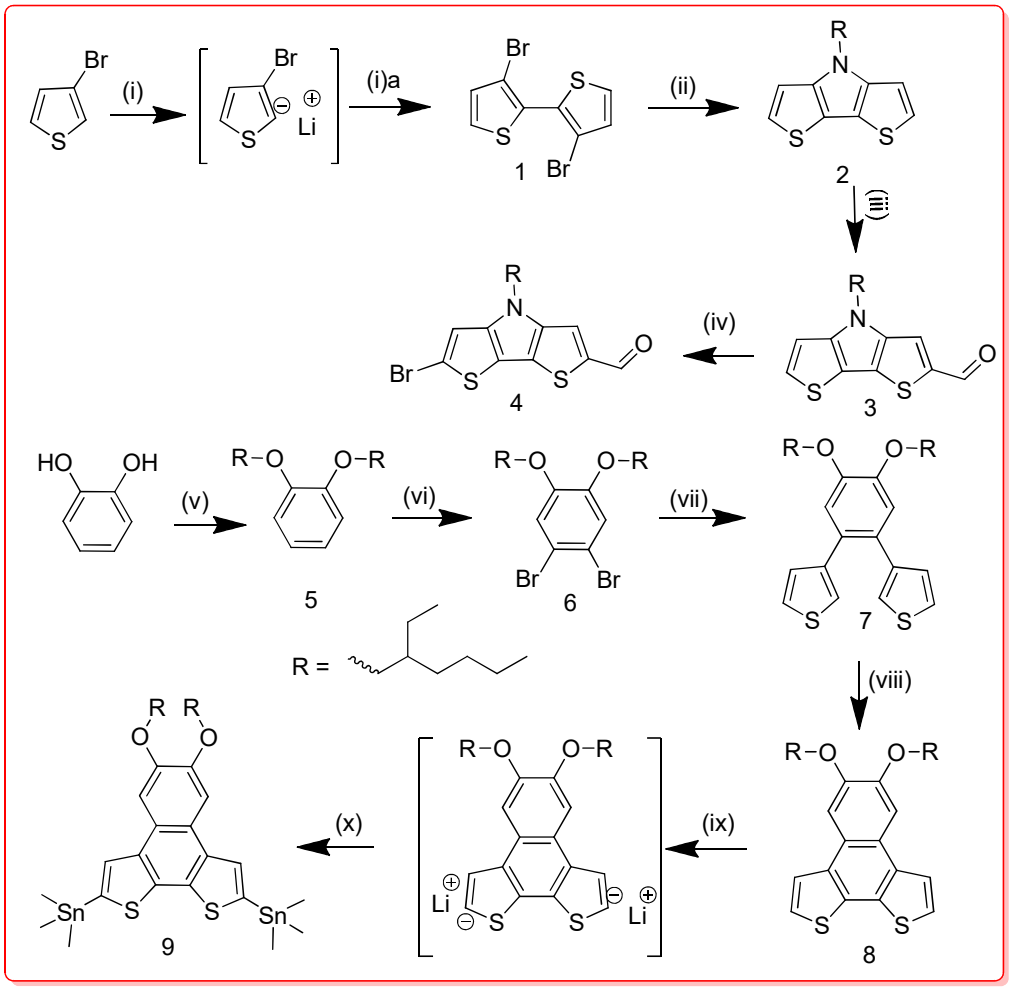

Scheme 5.2 Outline of synthetic scheme for intermediates **1-8**

Reagents and conditions: (i) n-BuLi, -78 °C, THF, (i)a $CuCl_2$, aqueous HCl, 70% (ii) 2-Ethyl hexyl amine, Sodium *tert*.butoxide, BINAP, $Pd_2(dba)_3$, Toluene reflux, 12h, 90% (iii) $POCl_3$, DMF, (Vilsmeier–Haack reaction), RT, 12h 76% (iv) NBS, 0 °C, THF, 12h 93% (v) EtOH, KOH, $C_8H_{17}Br$, 88%, (vi) NBS, $CHCl_3$/AcOH, 86%, (vii) tributyl(thiophen-3-yl)stannane, $Pd(PPh_3)_4$, Toluene, reflux, 12h, 84%, (viii) $FeCl_3$, $MeNO_2$, DCM, 78%, (ix) n-BuLi, -78 °C, THF (x) Me_3SnCl, 94%.

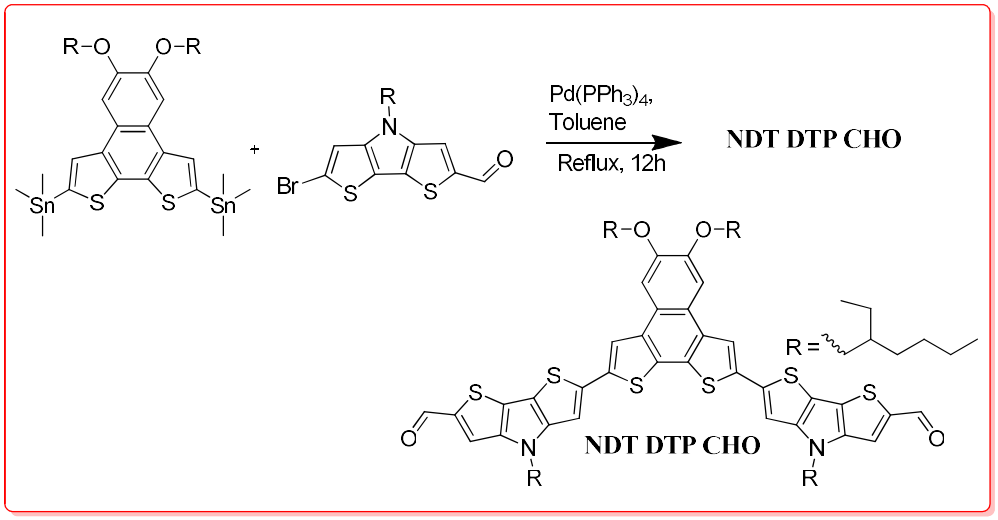

Scheme 5.3 Synthetic route for the preparation of dialdehyde intermediate

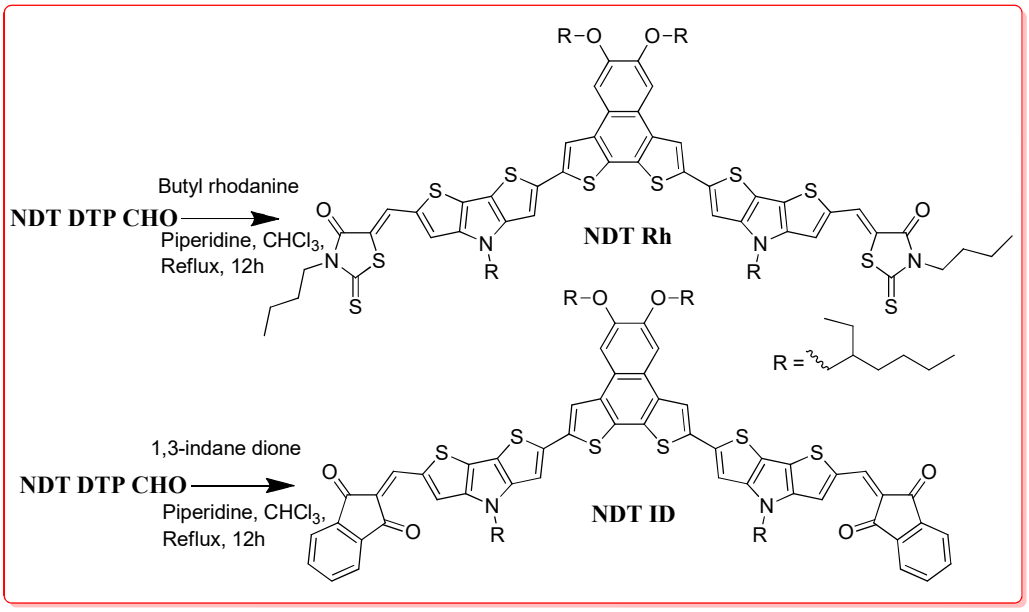

Scheme 5.4 Synthetic route for the target compounds (**NDT Rh** and **NDT ID**)

The absorption of **NDT Rh** from 350 nm to 700 nm, with a maximum absorption peak at 593 nm, and molar extinction coefficient 145070 ε , M^{-1} cm^{-1}. Compare with **NDT Rh, NDT ID** exhibits red shifted (34 nm) absorption maxima due to the better intra molecular charge transfer between the donor and acceptor (NDT DTP to 1,3-indanedione). **NDT ID** exhibit absorption at 627 nm with high molar extinction

coefficient i.e. 175973 ε , M^{-1} cm^{-1}. Fluorescence emission spectra of the donor materials were recorded in $CHCl_3$ solution ($1x10^{-5}$ M) and the results are summarized in Table 5.1. Two compounds show emission spectra at 677 nm and 701 nm for **NDT Rh** and **NDT ID** respectively. The optical band gap was calculated by following formula $1240/\lambda_{edge}$ (λ_{edge} = intersection point of absorption and Fluorescence). Optical band gap of **NDT Rh** is 1.92, and **NDT ID** is 1.84.

Table 5.1 Absorption (λ_{abs} in nm), molar extinction coefficient (ε), emission and optical band gap of **NDT Rh**, and **NDT ID**

Compound code	λ_{max} (nm)	Absorption maximum (ε, M^{-1} cm^{-1})	λ_{fluo} (nm)	Optical band gap (eV)
NDT Rh	408, 593	145070	677	1.92
NDT ID	427, 627	175973	701	1.84

NDT Rh and **NDT ID** compounds shows irreversible oxidation potentials and the oxidation potentials are 0.51 and 0.55 eV based on following oxidation potentials **NDT Rh** and **NDT ID** possess HOMO energy levels are -5.21 and -5.25 eV, and they are good HOMO energy levels and suitable donor materials for SMOSCs. The LUMO energy levels are calculated using following equation $E_{LUMO} = E_{HOMO} + E_g^{opt}$. Based on the equation **NDT Rh** and **NDT ID**, LUMO energy levels are -3.29 and -3.41 eV

Table 5.2 Oxidation potential (E_{ox}), reduction potential (E_{red}), HOMO, LUMO energy levels of **NDT Rh** and **NDT ID.**

Compound code	(volts)[a]	HOMO[b]	LUMO[c]	ΔE_g^{opt} [d](eV)
NDT Rh	0.51	-5.21	-3.29	1.92
NDT ID	0.55	-5.25	-3.41	1.84

Thermal stability of organic solar cell materials is most important when solar cells prepared by vacuum-deposition technique at high temperatures. Therefore, we investigated thermal decomposition by Thermo-gravimetric analysis (TGA) technique under a nitrogen atmosphere at a heating rate of 10 ℃ per minute. **NDT Rh** decomposes at 407 ℃, and **NDT ID** decomposes at 384 ℃ representing by they are suitable for vacuum-deposition technique.

The representative data are summarized in **Table 5.3**. This observation indicates good thermal stability of these materials even at high temperatures, required for vacuum deposition.

Table 5.3 Thermal data of the compounds

Compound code	T_d [a] (℃)
NDT Rh	407
NDT ID	384

[a] T_d: decomposition temperature (corresponding to 5% weight loss).

Two new donor materials **NDT Rh** and **NDT ID** were designed and synthesized for small molecule bulk hetero junction solar cell applications (SMBHJSCs). Optical, electro chemical and thermal properties of donor materials explored. To the best of our knowledge, for the first time naphtho[2,1-b:3,4-b']dithiophene (NDT) used as a donor material in small molecules due to it large planar conjugated system which delocalize the π-electrons and facilitates the efficient charge transfer through a NDT based bridge, two branched alkoxyl chains which increase the solubility of donor molecule. Two donor materials perform broad absorption in the UV-Visible region (350 nm-725 nm) with high molar extinction coefficients. Their HOMO/LUMO energy levels (-5.21/-3.29 eV for **NDT Rh** and -5.25/-3.41 eV for **NDT ID**) are well matched with **PCBM** acceptor (HOMO/LUMO energy levels of **PCBM** -6.0/-3.9 eV). Thermal decomposition of donor materials **NDT Rh** and **NDT ID** are 407 ℃ and 384 ℃ respectively and they are suitable for vacuum deposition fabrication technique. **NDT Rh** and **NDT ID** are showing promising properties for application in SMBHJSCs.

Chapter 6

Non-fullerene acceptors are most promising building blocks for organic bulk hetero junction solar cells (OBHJSCs). Generally, organic photovoltaic cells are containing a donor (p-type semiconductor) and an acceptor (n-type semiconductor) as active layer. n-type semiconductor are fullerene derivatives such as phenyl-C_{61}-butyric acid methyl ester ($PC_{61}BM$) and phenyl-C_{71}-butyric acid methyl ester ($PC_{71}BM$), and the power conversion efficiency's (PCEs) of p-type donors with fullerene derivatives reaching ≥11%. Last few decades $PC_{61}BM$, $PC_{71}BM$ fullerenes are widely used as an electron acceptor due to (i) the ability to accept and transport electrons (ii) high electron mobilities, (iii) multiple reversible electrochemical reductions, and (iv) the ability to aggregate in bulk heterojunctions to form both pure and mixed domains of the appropriate length scale for charge separation. But fullerene derivative acceptors having some drawbacks such as weak absorption in solar spectrum which leads to limited ability to harvest photocurrent, high synthetic costs, and instability of fullerenes. To overcome the disadvantages of fullerenes, much research focused on development of non-fullerene acceptors due to their enormous benefits like good and efficient light absorption in the visible, and near IR region, facile synthesis, fine-tuned energy levels by alter the molecular backbone and low cost, which have drawn high attention in OSCs most recently.

In this chapter we designed and synthesized two new non-fullerene acceptors **BDT Tz Rh** and **BDT DPP Rh**, A-D-A and A-A'-D-A'-A, architecture for OBHJSCs applications. Both acceptors having common donor benzo[1,2-b:4,5-b′]dithiophene (BDT) variant in alkyl chain (alkoxy side chain for **BDT Tz Rh** and thienyl alkyl chain for **BDT DPP Rh**) and butyl rhodhanine acceptor, by varied in thiazole spacer to electron acceptor moiety diketopyrrolopyrrole to evaluate the structure property relationship on optical, electrochemical and thermal properties.

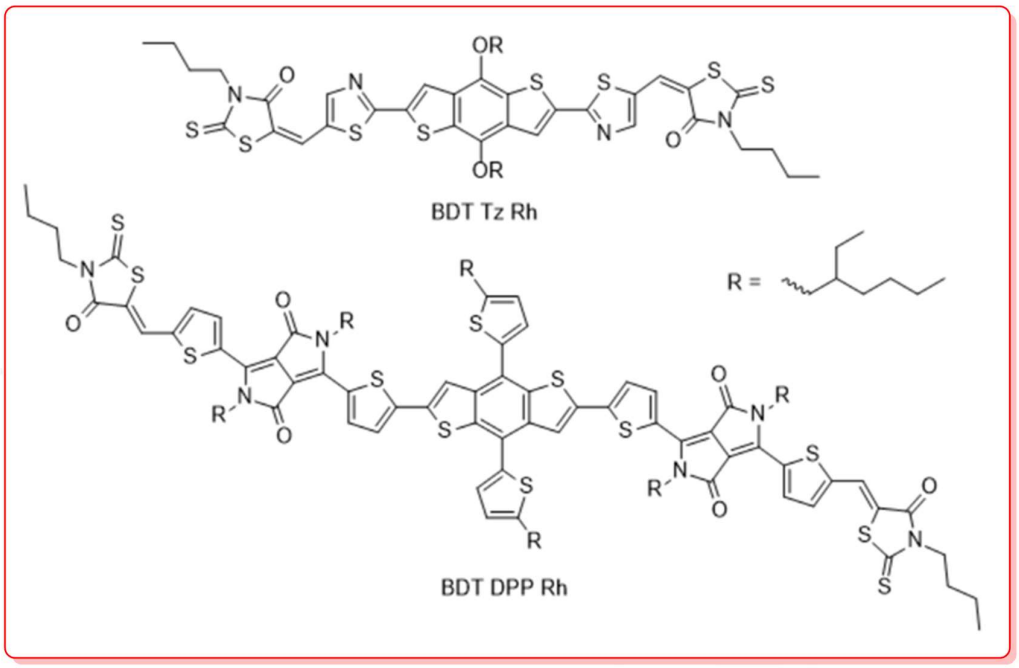

Scheme 6.1 Chemical structures of the two new **BDT** based fullerene free acceptors

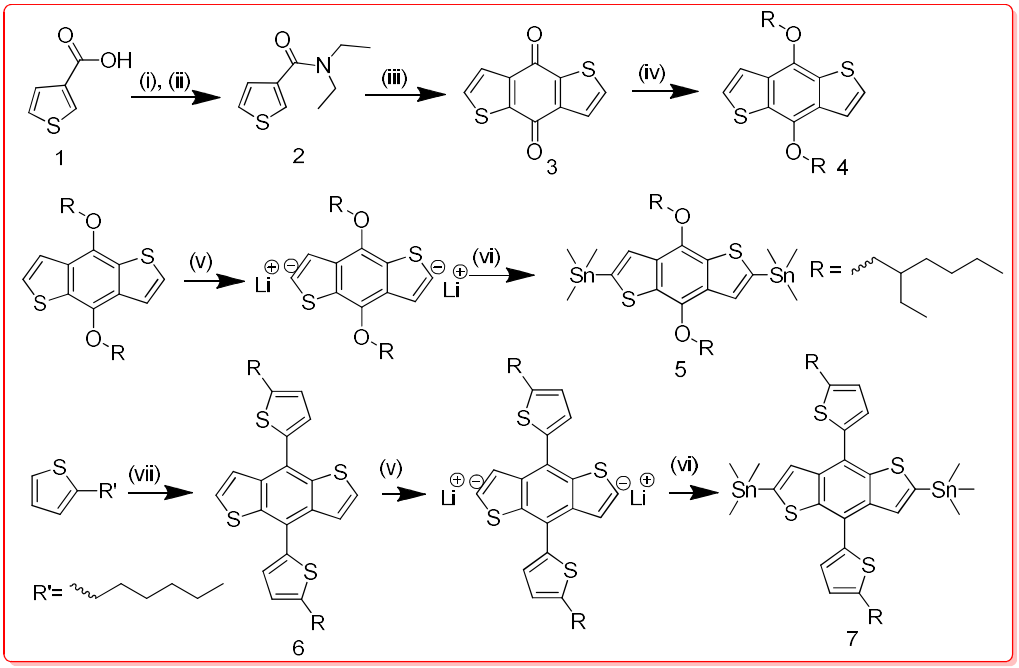

Scheme 6.2 Synthetic route for the preparation of **BDT** (**5** and **7**) intermediates

Reagents and conditions: (i) $(COCl)_2$, (ii) Diethylamine, (iii) THF, n-BuLi, -78°C, (iv) Zn, 50%NaOH, 2-EthylHexylbromide, (v) n-BuLi, -78°C, (vi) Tri Methyl Tin Chloride, (vii) (a) n-BuLi, -78°C, then Reflux 1h, (b) 3, reflux 1h, (c) $SnCl_2$+HCl+H_2O.

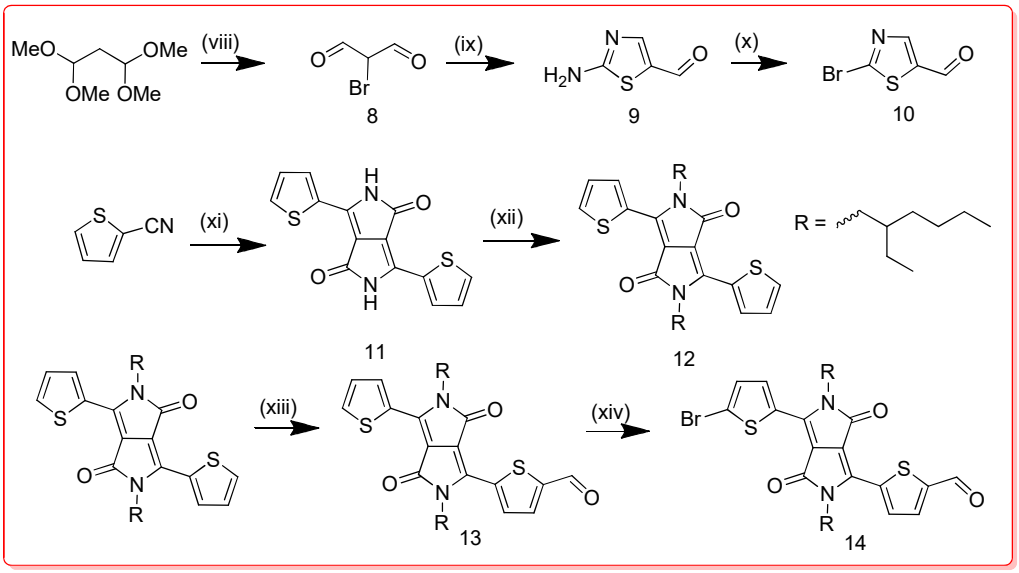

Scheme 6.3 Synthetic route for the preparation of **10** and **14** intermediates

Reagents and conditions: (viii) H_2O + HCl, 3h, Br_2, 2h (ix) H_2O, Thiourea, RT, 72h, (x) $CuBr_2$, Isopentylnitrite (xi) dibutyl succinate, Na, tert-amyl alcohol, 90 °C, 20 h (xii) 2-ethylhexyl bromide, DMF, K_2CO_3, 120 °C, 12 h (xiii) $POCl_3$, DMF 1,2 dichloroethane 12h (xiv) NBS, $CHCl_3$, 2h.

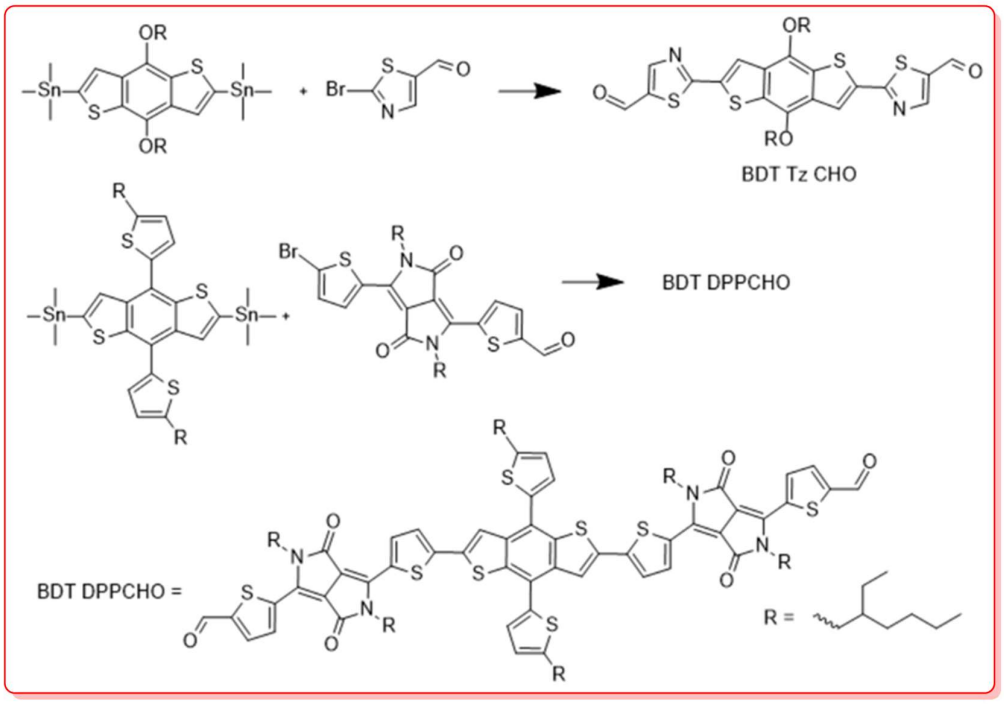

Scheme 6.4 Synthetic route for the key intermediates **BDT Tz CHO** and **BDT DPP CHO**

Reagents and Conditions: $Pd(PPh_3)_4$, Toluene, reflux, 12h.

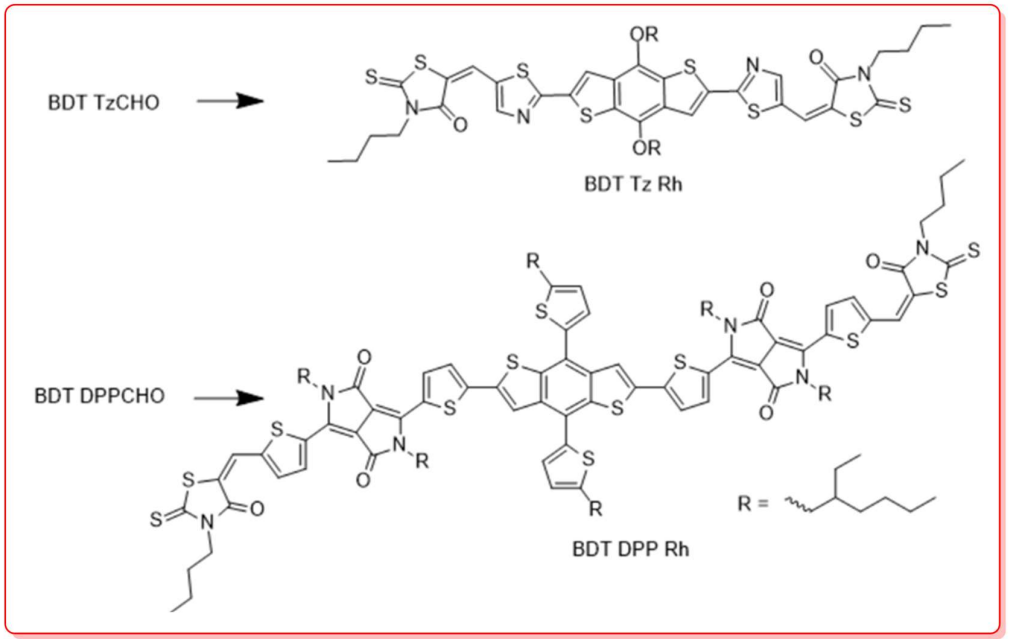

Scheme 6.5 Synthetic route for the target compounds **BDT Tz Rh** and **BDT DPP Rh**
Reagents and Conditions: Piperidine, Chloroform, reflux, 12h.

The UV–Visible absorption spectra of two new fullerene acceptors were recorded in $CHCl_3$ solution (10^{-5} M), and the results are summarized in Table 6.1. All the compounds exhibited two main absorption peaks, one ultraviolet (300 to 400 nm for **BDT Tz Rh** and 300-500 nm for **BDT DPP Rh**) and other in visible (400-650 nm for **BDT Tz Rh** and 500-800 for **BDT DPP Rh**) region. The red-shifted and stronger absorption of the **BDT DPP Rh** can be attributed to the elongated p-conjugation length and strengthened ICT effect. Fluorescence intensity of **BDT Tz Rh** and **BDT DPP Rh** are 671 and 764 respectively.

Table 6.1 Absorption (λ_{abs} in nm), molar extinction coefficient (ε), and emission maximum (λ_{fluo}) of small molecules recorded in chloroform**.**

Compound code	λ_{abs} **(nm)**	**Molar extinction coefficient (ε), (L M^{-1} cm^{-1})**	λ_{fluo} **(nm)**	**Optical band gap (E_g^{opt})**
BDT Tz Rh	460, 510, 538	179035, 161435, 166935	671	2.12
BDT DPP Rh	656, 711	79348, 91542	764	1.67

The electrochemical properties were investigated in an electrolyte consisting of a solution of 0.1M tetrabutylammonium perchlorate (n-Bu_4NClO_4) in anhydrous CH_2Cl_2 at room temperature under nitrogen with a scan rate of 50mV/s and ferrocenium/ ferrocene redox couple was used as an internal reference. The HOMO/LUMO energy levels of the derivatives were calculated using onset oxidation/onset reduction potential following the equation: HOMO = E_{ox}^{onset} + 4.7 eV, LUMO = E_{HOMO} + $\boldsymbol{E_g^{opt}}$ eV. The cyclic voltammograms of the synthesized **BDT** based acceptors were depicted in Figure **3** and reduction potential, HOMO, LUMO, and optical band gap values were summarized in Table **6.2**.

Table 6.2 Oxidation potential (E_{ox}), HOMO, LUMO and optical band gap (E_g^{opt})) of the compounds.

Comp code	E_{ox}^{onset} (volts)[a]	HOMO[b]	LUMO[c]	$E_g^{opt\ d}$ (eV)
BDT Tz Rh	1.00	-5.70	-3.58	2.12
BDT DPP Rh	0.80	-5.50	-3.83	1.67

High thermal stability is an important requirement for the materials for practical applications. Therefore, thermal properties of the synthesized donor materials were investigated using thermogravimetric (TG) analyses. TGA curves of these donor materials and the corresponding data are provided Table **6.3**, Both **BDT Tz Rh** and **BDT DPP Rh** have excellent thermal stability with the decomposition temperatures (T_d, defined as that at which 5 wt % loss is observed) 354 ℃ and 395 ℃, respectively for **BDT Tz Rh** and **BDT DPP Rh**).

Table 6.3 Thermogravimetric (TG) analyses data of synthesized compounds.

Compound Code	T_d (℃)
BDT Tz Rh	354.8
BDT DPP Rh	395.2

[a]T_d: decomposition temperature (corresponding to 5% weight loss).

In this chapter we design and synthesized two new non-fullerene acceptor materials named **BDT Tz Rh** and **BDT DPP Rh** for OPVs. All the materials **BDT Tz Rh** and **BDT DPP Rh** exhibited wide and efficient absorption in visible region with high molar extinction coefficient, and they are soluble in common organic solvents like $CHCl_3$ (**BDT Tz Rh** 10 mg/mL and **BDT DPP Rh** 40 mg/mL). **BDT Tz Rh** exhibited absorption up to 650 nm and the energy levels 5.70/-3.58 eV. This material used for non-fullerene acceptor for variety of donor materials which are having higher absorption like **PTB7** (650 nm and above) and suitable HOMO/LUMO energy levels. **BDT DPP Rh** exhibited strong and efficient absorption in visible-IR region (up to 800

nm). The red-shifted and stronger absorption of the **BDT DPP Rh** can be attributed to the elongated p-conjugation length and strengthened ICT effect. **BDT DPP Rh** having lower LUMO energy levels than the **BDT Tz Rh** due to the strong **DPP** acceptor unit. Most of the polymer/small molecule donor molecules exhibited absorption up to 700 nm. **BDT DPP Rh** is a good choice to use an acceptor for polymer/small molecule donors (which is having absorption up to 700 nm) because when fabricated with donor material the solar cell device absorbs entire solar flux from solar spectrum which is help full to increase the short circuit current (J_{SC}).